A New Protection Strategy for Grid-Forming Renewable Power Outgoing Lines Using Characteristic Signal Amplitude Ratio

Yawei Li *, Chao Xie, Junru Chen, Muyang Liu, Chunya Yin

Posted Date: 28 February 2026

doi: 10.20944/preprints202602.2045.v1

Keywords: grid-forming; outgoing line; longitudinal protection; active detection

 doi:10.20944/preprints202602.2045.v1

Article

A New Protection Strategy for Grid-Forming Renewable Power Outgoing Lines Using Characteristic Signal Amplitude Ratio

Yawei Li *, Chao Xie, Junru Chen, Muyang Liu and Chunya Yin

College of Electrical Engineering, Xinjiang University, Urumqi 830017, China
* Correspondence: 107552304608@qq.com

Abstract

Grid-forming (GFM) renewable energy sources are increasingly integrated into power grids to enhance the stability of high-penetration renewable energy systems, while the fault current characteristics of GFM-based outgoing lines lead to the inapplicability of conventional longitudinal differential protection, which suffers from reduced sensitivity or even refusal to operate under weak grid conditions. To address this issue, this paper proposes a novel active detection-based protection strategy for GFM photovoltaic power station outgoing lines based on the amplitude ratio of characteristic harmonic signals. First, the sequence equivalent circuits of the GFM system during grid faults are established to analyze the fault current characteristics, and the inapplicability mechanism of conventional pilot differential protection is revealed. Considering the filter cutoff frequency, harmonic interference avoidance and power quality constraints, the 8th harmonic is selected as the characteristic signal, and a proportional-resonant (PR) controller is adopted to realize the independent and flexible injection of the characteristic signal and power frequency signal. Based on the distribution difference of characteristic signals under internal and external faults, a protection criterion is constructed using the amplitude ratio of the harmonic component of the differential current to the characteristic signal injected on the station side. The simulation results on the MATLAB/Simulink platform show that the proposed strategy can quickly and accurately distinguish various internal and external faults of the transmission line, and operate reliably under different fault types, fault locations and high transition resistance.

Keywords: grid-forming; outgoing line; longitudinal protection; active detection

1. Introduction

To achieve global carbon neutrality, inverter-interfaced renewable energy sources such as photovoltaic and wind power have been increasingly integrated into modern power systems[1]. This transformation has fundamentally altered grid fault characteristics and posed significant challenges to conventional relay protection schemes [2]. As a representative advanced control strategy, GFM control enables renewable energy inverters to operate as voltage sources, providing autonomous voltage and frequency support and effectively enhancing the transient stability of power systems with high renewable penetration [3]. Consequently, GFM control is expected to become the dominant operating mode of future renewable energy power stations.

Most existing studies have focused on GFM control strategies, fault current limiting, and system stability analysis. However, during grid faults, the fault characteristics of GFM converters differ from those of grid-following (GFL) converters and traditional synchronous generators (SG) [4], leaving the operational reliability of traditional relay protection schemes still confronted with significant

 doi:10.20944/preprints202602.2045.v1

challenges. Therefore, there is an urgent need to explore novel protection principles tailored for AC outgoing lines in large-scale power evacuation scenarios of GFM-based renewable energy units.

At present, some scholars have conducted preliminary analyses on the applicability of traditional protection in grid-connected systems of the network type. Reference [5] qualitatively analyzed the applicability of conventional protection and transient quantity protection in grid-connected systems with GFM inverters, pointing out that the increase in GFM penetration will pose challenges to the sensitivity and reliability of protection devices. Reference [6] indicated that GFM converters are more conducive to the operation performance of conventional protection compared with GFL ones, yet it failed to investigate the applicability of conventional protection under weak grid conditions. Reference [7] established the three-sequence equivalent circuit of the GFM-based outgoing transmission line system and found that the amplitude and phase of fault current are significantly affected by fault conditions, voltage drop degree and control strategies. Reference [8] analyzed the failure problem of conventional distance protection under the control of virtual synchronous machines and proposed a corresponding improved control strategy. Reference [98] explored the fault sequence current characteristics of GFM converters and put forward a pilot protection principle based on composite sequence current for GFM-based outgoing lines, while the applicability of conventional protection in this scenario remains unspecified. Reference [10] proposed a protection principle for GFM-based outgoing lines based on current waveform similarity; however, this method has high requirements for waveform quality, is susceptible to phase angle distortion on the renewable energy side, and suffers from insufficient sensitivity. Reference [11] proposed a high-frequency signal-based active protection scheme for outgoing lines, which can identify fault types and fault natures but is limited by poor economic efficiency. Reference [12–15] proposed a protection idea of actively injecting characteristic signals through inverters during line faults. Although such methods are mostly applied in distribution network scenarios, their research ideas provide an important reference for the development of new protection principles for GFM-based renewable energy outgoing lines.

To overcome these limitations, this paper proposes a novel active detection-based protection strategy for GFM photovoltaic power station outgoing lines based on the amplitude ratio of characteristic harmonic signals. The main contributions of this paper are as follows: (1) Sequence equivalent circuit models of GFM photovoltaic systems under fault conditions are established, and the positive-, negative-, and zero-sequence fault current characteristics are analyzed to elucidate the failure mechanism of conventional longitudinal current differential protection; (2) A multi-constraint characteristic harmonic selection method is developed, and the 8th harmonic is selected as the optimal characteristic signal by comprehensively considering filter bandwidth, harmonic interference avoidance, power quality constraints, and signal extraction feasibility. A PR controller-based injection strategy is further designed to enable decoupled control of power-frequency and characteristic harmonic components; (3) The distribution behavior of the injected 8th harmonic under internal and external faults is investigated, and an amplitude ratio-based protection criterion is formulated to improve the robustness to harmonic interference and high transition resistance; (4) Extensive MATLAB/Simulink simulations are conducted to verify the effectiveness and superiority of the proposed protection strategy under different fault types, fault locations, and transition resistances.

2. Materials and Methods

This study focuses on the grid-connected renewable energy photovoltaic (PV) power station controlled by a virtual synchronous generator (VSG). The typical topological structure of the AC outgoing lines and the grid-connected control structure of this type of power station are shown in Figure 1.

 doi:10.20944/preprints202602.2045.v1

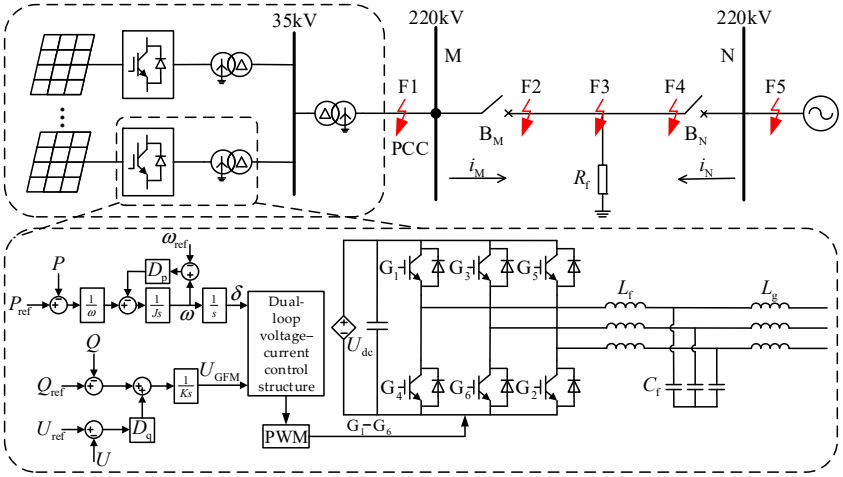

Figure 1. Topology and control structure of GFM PV power station outgoing lines. The region enclosed by the dashed box depicts the control structure schematic of the VSG. Where line MN is the outgoing line for new energy, BM and BN are the protection on the side of the new energy power station and the system side respectively, F2-F4 are faults within the outgoing line area, F1 and F5 are faults outside the outgoing line area, U_{dc} is a DC voltage source is employed to simulate renewable energy sources, G1-G6 are the switching tube of the three-phase full-bridge converter, L_f, C_f and L_g represent the filter inductor, filter capacitor and line inductor, respectively.

2.1 Analysis of Fault Characteristics of Outgoing Lines for Grid-Forming Renewable Power

Although the fault characteristics of GFM inverter-interfaced power sources differ from those of SG-based power sources, the fault boundary conditions at the fault location remain unchanged. Consequently, their sequence component relations are consistent with those of faults in traditional AC outgoing lines [16]. The connection relations of each sequence network under different fault types still adhere to the basic principles of the symmetrical component method; however, the short-circuit current sequence component characteristics they provide to the power system are fundamentally distinct from those of synchronous generators. This difference primarily originates from the control strategies and current-limiting measures of GFM inverters. The sequence equivalent circuits of the grid-forming renewable energy system during line faults are illustrated in Figure 2.

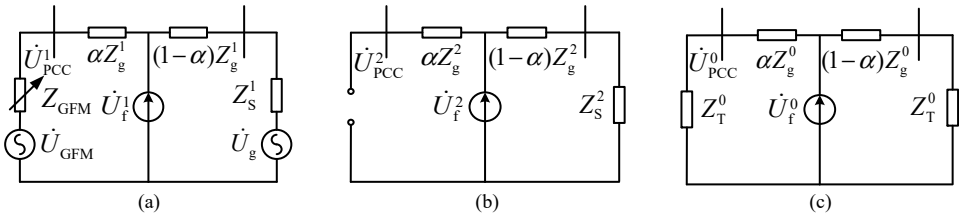

Figure 2. Equivalent circuit of grid-forming renewable power stations during grid faults (a) Positive-sequence equivalent network; (b) Negative-sequence equivalent network; (c) Zero-sequence equivalent network.

This paper analyzes the LVRT strategy based on virtual impedance current limiting. At this point, the positive-sequence network can be equivalently modeled as a voltage source in series with a variable impedance, which is related to the positive-sequence voltage sag severity at the grid connection point [5]. In practical engineering applications, to mitigate current distortion under unbalanced conditions and enhance the stability of system operation, GFM renewable energy power stations usually adopt a negative-sequence current suppression strategy, with the negative-sequence current reference value set to zero. When the power grid experiences asymmetric faults that introduce negative-sequence voltage components, this strategy forces the station-side negative-sequence current to be approximately zero. Consequently, the negative-sequence network of GFM renewable energy power stations can be equivalently regarded as an open circuit. GFM inverters lack the

 doi:10.20944/preprints202602.2045.v1

capability to independently generate zero-sequence voltage in terms of their topological structure and modulation scheme, and GFM renewable energy power stations themselves do not supply zero-sequence current to the power system. From the aforementioned analysis, it can be concluded that regardless of the fault type occurring on the transmission line, the short-circuit current supplied by GFM renewable energy power stations only contains positive-sequence components. When a fault occurs on the outgoing line, GFM inverter-interfaced power sources under VSG control still maintain their pre-fault operating state at the fault instant, owing to the fact that the time scale of the power control loop is slower than that of the current inner loop. To simplify the analysis process, it is assumed that the amplitude and phase of the converter electromotive force (EMF) remain constant within a short time interval following fault occurrence [4]. Based on the positive-sequence equivalent circuit, the steady-state fault current can be derived [8]:

$$\dot{I}_{GFM} = \frac{\Delta\dot{U}}{Z_{GFM}} = \frac{\dot{U}_{GFM} - \dot{U}^{1}_{PCC}}{R_{GFM} + jX_{GFM}} = \left|\dot{I}_{GFM}\right| e^{j\theta} \tag{1}$$

$$\begin{cases} \left|\dot{I}_{GFM}\right| = \sqrt{I_d^{+2} + I_q^{+2}} \\ \theta = \theta^{+}_{PCC} - \varphi \\ \varphi = \arctan\left(-I_q^{+} / I_d^{+}\right) \\ I_d^{+} = \dfrac{\mathrm{Re}[\Delta\dot{U}]R_{GFM} + \mathrm{Im}[\Delta\dot{U}]X_{GFM}}{R_{GFM}^2 + X_{GFM}^2} \\ I_q^{+} = \dfrac{\mathrm{Im}[\Delta\dot{U}]R_{GFM} - \mathrm{Re}[\Delta\dot{U}]X_{GFM}}{R_{GFM}^2 + X_{GFM}^2} \end{cases} \tag{2}$$

Where $\dot{U}_{GFM}$ is the equivalent internal EMF of the GFM photovoltaic power station; $\dot{U}^{1}_{PCC}$ is the positive-sequence voltage at the grid connection point at the fault instant; Z_{GFM} is the virtual impedance; R_{GFM} and X_{GFM} are the virtual resistance and virtual reactance, respectively, including the impedance between the internal EMF before the fault and the grid connection point; θ^{+}_{PCC} is the phase angle of the positive-sequence voltage at the grid connection point after the fault; φ is the power factor angle.

From Equation (2), It is inferred that the amplitude and phase angle of the positive-sequence short-circuit current supplied by GFM renewable energy power stations are related to the phase angle of the positive-sequence voltage at the grid connection point, the positive-sequence voltage sag severity, as well as the power factor angle after the virtual impedance is activated.

2.2 Applicability Analysis of Conventional Pilot Differential Protection for Outgoing Lines

Generally, for renewable energy AC outgoing lines, the main protection adopted remains pilot differential protection. Conventional current differential protection utilizes the amplitude and phase relationships of the power frequency current phasors at both ends of the protected line for fault identification. The ratio braking-type operating equation is expressed as Equation (3).

$$\left|\dot{I}_M + \dot{I}_N\right| > K\left|\dot{I}_M - \dot{I}_N\right| \tag{3}$$

Where $\dot{I}_M$ and $\dot{I}_N$ denote the fundamental frequency current phasors at the renewable energy side and the system side of the GFM renewable energy outgoing line, respectively; $\left|\dot{I}_M + \dot{I}_N\right|$ is the differential current; $\left|\dot{I}_M - \dot{I}_N\right|$ is the braking current; K is the braking coefficient setting value of the main criterion, which is typically set in the range of 0.5 to 0.8. Let $\dot{I}_M / \dot{I}_N = \rho$,then Equation (3) can be rearranged as

$$\left|\rho + 1\right| > \left|\rho - 1\right| \tag{4}$$

When GFM renewable energy power stations are integrated into a strong power grid, the system-side short-circuit current can reach dozens of times the rated current; even when connected to a weak power grid, the system-side short-circuit current can still reach 2 to 3 times the rated current.

 doi:10.20944/preprints202602.2045.v1

Under such circumstances, $|\rho| < 1$,a unit circle can be constructed with the system-side short-circuit current as the reference, as illustrated in Figure 3. This circle corresponds to the operating characteristics of pilot differential protection in the amplitude-phase plane, where the shaded area inside the circle denotes the braking zone of pilot differential protection [17]. Consequently, the amplitude and phase relationships of the short-circuit currents at both ends of the transmission line can be characterized by a single point on this unit circle under all operating conditions and fault types.

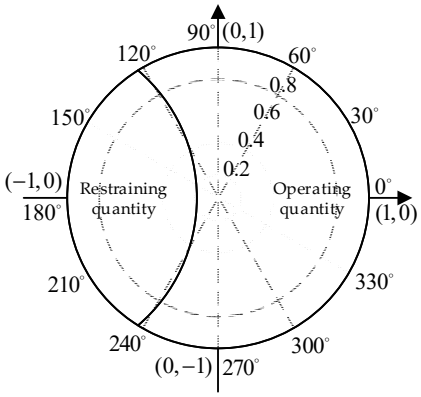

Figure 3. Operational characteristics of braking Criterion on the amplitude-phase plane.

From the analysis presented in Section 2.1, It is inferred that the phase of the short-circuit current output by the GFM renewable energy power station is related to the phase angle and sag severity of the positive-sequence voltage at the grid connection point, as well as the power factor angle after the virtual impedance is activated. Consequently, the phase relationship of the short-circuit currents at both ends of the transmission line cannot be determined following a fault. When a GFM renewable energy power station is integrated into a strong power grid, the amplitude difference of the short-circuit currents at both ends of the line is significant, ρ will fall near the center of the unit circle, leading to a reduction in the sensitivity of the pilot differential protection. In contrast, when the GFM renewable energy power station is connected to a weak power grid, the amplitude difference of the short-circuit currents at both ends of the line is negligible, ρ will fall near the boundary of the unit circle. Under such circumstances, the operating performance of the pilot differential protection is determined by the phase difference between the short-circuit currents at both ends of the line. Due to the uncertainty in the phase of the short-circuit current on the station side, the protection may fail to operate during an internal fault.

In summary, to address the issues where the sensitivity of the pilot current differential protection decreases when GFM renewable energy power stations are integrated into a strong power grid and the pilot differential protection fails to operate when connected to a weak power grid, this paper leverages the flexibility and controllability of GFM renewable energy power stations, adopts orthogonal control with the power frequency controller, and injects characteristic signals into the power system through the GFM inverter. By investigating the differences in the system's response to the injected characteristic signals, a novel protection method and its implementation scheme are proposed.

3. Selection of Characteristic Signals and Injection Methods

3.1. Initiation Criterion for Characteristic Signal Injection

At the instant a system fault occurs, the positive-sequence voltage at the grid connection point of the GFM renewable energy power station experiences a sag, with a significant decrease in its amplitude. The characteristic of the positive-sequence voltage amplitude sag at the grid connection point can be employed as one of the initiation criteria for characteristic signal injection. When an

 doi:10.20944/preprints202602.2045.v1

asymmetric fault occurs within the power system, the amplitude of the negative-sequence voltage at the grid connection point still exhibits a significant increase; similarly, the amplitude characteristic of the negative-sequence voltage can be utilized as another initiation criterion for characteristic signal injection. Figure 4 illustrates the variations in the positive-sequence and negative-sequence voltages at the grid connection point on the power station side when different types of faults occur at the internal fault point F3.

In this paper, the sudden change characteristics of the positive-sequence and negative-sequence voltages at the grid connection point of the GFM renewable energy power source are adopted as the initiation criteria for signal injection. Specifically, the positive-sequence voltage at the grid connection point $u_1(i)$ is monitored, and the sudden change in the positive-sequence voltage at the grid connection point, $\Delta u_1(i)$ is calculated as shown in Equation (4).

$$\Delta u_1(i) = \left| u_1(i) - u_1(i-k) \right| \tag{5}$$

$$\Delta u_1(i) > \Delta u_{1.set} \tag{6}$$

Similarly, the negative-sequence voltage at the grid connection point $u_2(i)$ is monitored, and the sudden change in the negative-sequence voltage at the grid connection point, $\Delta u_2(i)$ is calculated as shown in Equation (5).

$$\Delta u_2(i) = \left| u_2(i) - u_2(i-k) \right| \tag{7}$$

$$\Delta u_2(i) > \Delta u_{2.set} \tag{8}$$

Where i denotes the current sampling instant, $i-k$ denotes the k-th previous sampling instant; $\Delta u_{1.set}$ and $\Delta u_{2.set}$ denote the sudden change thresholds of the positive-sequence voltage and negative-sequence voltage at the grid connection point, respectively. These thresholds are set based on the voltage fluctuation of the power system under maximum disturbance, with a certain margin considered [18], $\Delta u_{1.set} = \Delta u_{2.set} = 1.2(3\%U_N)$.

If all consecutive sampling points satisfy either Equation (6) or Equation (8), it indicates that a fault has occurred within the power system, and the injection of the characteristic signal is initiated. k and N are adjustable according to engineering requirements, with $k = 1$ and $N = 7$ adopted in this study.

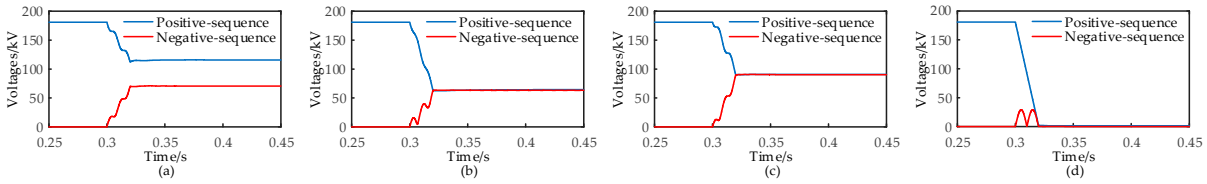

Figure 4. Positive-sequence voltage and negative-sequence voltage at the PCC during grid faults (a)AG; (b)ABG; (c)AB; (d)ABC/ABCG.

3.2. Selection of Characteristic Signals

In the design of the active detection-based protection method, appropriate control parameters for the characteristic signal must be selected to achieve stable injection of the characteristic signal current. The following analysis focuses on the selection of key parameters of the characteristic signal, including its frequency and amplitude.

3.2.1. Frequency Selection of the Characteristic Signal

Before being injected into the power grid, the characteristic signal must pass through the grid-connected filter of the GFM inverter. The cutoff frequency of the GFM inverter output filter is generally set within the range of 10 times the fundamental frequency to half the carrier frequency. Consequently, the frequency of the characteristic signal must be lower than 10 times the fundamental frequency to avoid resonance and signal attenuation [12]. When a transmission line fault occurs, GFM renewable energy power sources inevitably generate certain harmonic components, predominantly

 doi:10.20944/preprints202602.2045.v1

low-order harmonics (2nd to 4th order). To avoid interference from these low-order harmonics on the characteristic signal injected for protection purposes, the characteristic frequency should be higher than the main harmonic frequency generated by the GFM renewable energy power sources themselves [13]. Additionally, the harmonics passively output by GFM renewable energy power sources under system disturbances are mainly odd-order harmonics; to reduce the impact of transient odd-order harmonics in the power system on characteristic signal extraction, even-order harmonics should theoretically be selected as the system fault characteristic harmonics [14]. Furthermore, to reduce the computational complexity during spectrum analysis and minimize the signal processing time, selecting the characteristic signal frequency as an integer multiple of the fundamental frequency facilitates the rapid implementation of signal processing methods such as Fourier transform (FFT) [15].

Considering all the aforementioned constraints, and noting that a higher characteristic signal frequency enables the extraction of more characteristic values within the same data window length of the protection device, the 8th-order harmonic signal is selected as the injected characteristic signal in this paper to maximize the reliability of the protection scheme.

During the normal operation of the GFM renewable energy system, FFT analysis is performed on the harmonic characteristics of the grid connection point current after the injection of the characteristic signal, with the analysis results illustrated in Figure 5. The results indicate that the injected harmonic signal exerts no adverse impact on the system current quality, and the total harmonic distortion (THD) of the system current complies with the requirements of relevant grid-connection technical standards.

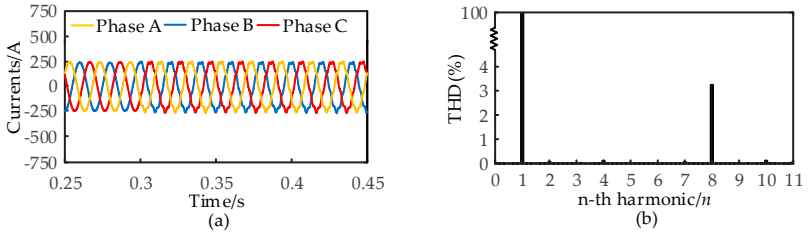

Figure 5. Three-phase PCC currents and FFT results after characteristic signal injection (a) Three-phase currents at the station side; (b) FFT of PCC currents after characteristic signal injection.

3.2.2. Amplitude Selection of the Characteristic Signal

The determination of the characteristic signal amplitude must comprehensively balance two key factors: the monitoring difficulty at the protection installation location and the power quality of the power grid. Specifically, considering the attenuation of the characteristic signal during its propagation along the transmission line, the harmonic content inherently generated by the system-side transient process, and the sampling and calculation accuracy of the characteristic signal at the protection installation location, the amplitude of the injected characteristic signal should not be excessively small. Meanwhile, to mitigate the impact of the characteristic signal on system power quality and ensure compliance with the current-carrying capacity of power electronic devices in the system, the amplitude of the injected characteristic signal should not be excessively large. With the constraints that the power quality at the grid connection point meets the standard requirements and the output current of all types of power electronic devices does not exceed their rated limits, the amplitude of the characteristic signal is set to 5% of the rated output current of the GFM power source under normal operating conditions in this paper [19].

3.3. Injection Method of the Characteristic Signal

Currently, GFM renewable energy control systems typically employ a proportional-integral (PI) controller to regulate the collected fundamental frequency signals, which are converted into DC signals via abc-dq coordinate transformation. The frequency response characteristic of the PI

 doi:10.20944/preprints202602.2045.v1

controller exhibits a high gain only for DC signals. In contrast, characteristic signals with frequencies far higher than the fundamental frequency do not have a zero frequency after coordinate transformation, rendering the PI controller ineffective in regulating these characteristic signals. On the other hand, the frequency response characteristic of the PR controller provides a high gain exclusively for signals at its designed operating frequency; thus, a PR controller not tuned to the fundamental frequency cannot effectively regulate fundamental frequency signals. In this paper, PR control is adopted as the underlying controller for the characteristic frequency current control loop to achieve rapid tracking of characteristic signal commands. The transfer function of the characteristic frequency control loop is given in Equation (9) [12].

$$G_{PR}(s) = K_p + \frac{K_r s}{s^2 + (2\pi f_h)^2} \tag{9}$$

Where K_p and K_r denote the proportional coefficient and resonant coefficient of the PR controller respectively; f_h is the operating frequency of the PR controller, which is consistent with the frequency of the injected characteristic signal. To achieve flexible control of the injected characteristic signal, the characteristic signal injection process and control structure adopted in this paper are illustrated in Figure 6.

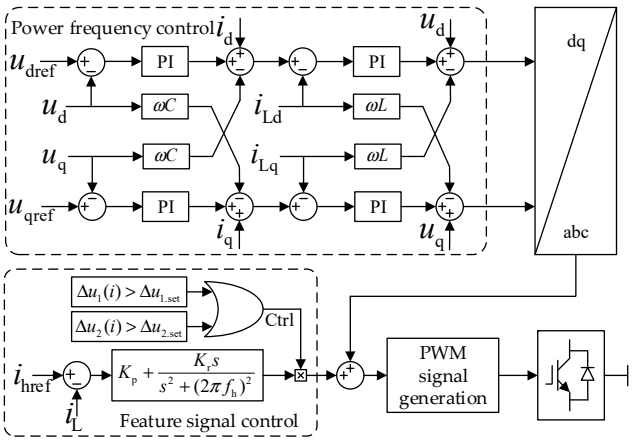

Figure 6. Injection Process of the Characteristic Signal. Ctrl is the enable signal generated by the characteristic signal injection startup criterion; i_{href} is the reference value of the characteristic frequency current.

To avoid the failure of characteristic signal injection, the amplitude of the 8th-order harmonic current at the station side is detected immediately after the characteristic signal injection startup criterion is satisfied. If the amplitude of the harmonic current measured at the station side fails to reach 3% of the rated output current of the GFM power source under normal operation within a continuous 10 ms , the injection process is restarted. If the aforementioned condition still fails to be met within another continuous 10 ms , the injection circuit is determined to be abnormal. In this case, the protection criterion is immediately blocked to prevent misjudgment caused by signal abnormalities.

4. Longitudinal Protection Based on the Amplitude Ratio of Characteristic Signals

4.1. Distribution Characteristics of Fault Characteristic Signals Inside and Outside the Protection Zone

Based on Figure 7, this paper analyzes the distribution characteristics of characteristic signals on both sides of the outgoing lines of the GFM renewable energy power station when internal and external faults occur on the lines.

 doi:10.20944/preprints202602.2045.v1

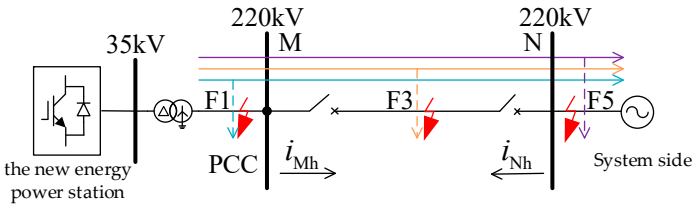

Figure 7. diagram of characteristic signal distribution for internal and external faults. F1 denotes an external fault on the station side of the outgoing line; F3 represents an internal fault on the outgoing line; and F5 indicates an ex-ternal fault on the system side of the outgoing line. and are the characteristic frequency currents measured on the station side and the system side, respectively.

When an internal fault occurs on the transmission line, the positive-sequence voltage at the PCC on the station side drops or the negative-sequence voltage rises, triggering the characteristic signal injection criterion. Subsequently, the GFM renewable energy power source injects the 8th-order harmonic characteristic signal into the transmission line. In the case of a metallic grounding fault, the injected harmonic current flows from the fault point to the ground and does not propagate to the opposite side of the line. Even if a transition resistance exists at the fault point, the fault point still diverts the harmonic current to a certain extent; thus, there is a significant difference in the proportion of characteristic harmonic currents flowing through the M-side and N-side of the transmission line.

When an external fault occurs on the station side of the transmission line, the characteristic signal injection criterion is normally activated, and the GFM renewable energy power source injects harmonic current into the line. Since the short-circuit currents flowing through the M-side and N-side of the line are both the through currents supplied by the system side, the amplitudes of the harmonic currents on both sides of the line are almost identical, with an overall relatively small amplitude.

When an external fault occurs on the system side of the transmission line, the characteristic signal injection criterion is still normally activated, and the GFM renewable energy power source injects harmonic current into the line. Since the short-circuit currents flowing through the M-side and N-side of the line are both the through currents supplied by the station side, the amplitudes of the harmonic currents on both sides of the line are almost identical, with an overall relatively large amplitude.

4.2. A New Criterion for Longitudinal Harmonic Current Protection

Based on the distribution characteristics of characteristic signals under internal and external faults, when an internal fault occurs on the transmission line, the amplitude of the harmonic current on the station side is significantly larger than that on the system side due to the shunting effect of the fault point on the injected harmonics. Considering that a small amount of transient harmonic components with relatively small amplitudes will be generated on the system side within one fundamental frequency cycle after the fault occurs, directly using the difference between the harmonic currents on both sides to set the operating threshold will make the protection prone to interference from these transient harmonics, leading to incorrect operation or operation delay. To further highlight the fault differences, this paper introduces the amplitude information of the harmonic current injected on the station side, and constructs a novel longitudinal protection criterion based on this information, thereby improving the reliability and sensitivity of the protection criterion.

The ratio of the amplitude of the short-circuit current harmonic component measured on both sides of the transmission line to the amplitude of the harmonic current injected on the station side is defined as the differential current harmonic ratio. When a fault occurs on the transmission line, the amplitude ratio of the harmonic component of the differential current on both sides to the harmonic component on the system side is first calculated, as given in Equation (10). The protection criterion is then constructed by comparing this amplitude ratio with the protection threshold, as presented in Equation (11).

 doi:10.20944/preprints202602.2045.v1

$$\lambda_{\varphi} = \frac{\left|\dot{I}_{\varphi M} + \dot{I}_{\varphi N}\right|_h}{\left|\dot{I}_{\varphi Mh}\right|} \tag{10}$$

$$\lambda_{\varphi} > \lambda_{set} \tag{11}$$

Where $\left|\dot{I}_{\varphi M} + \dot{I}_{\varphi N}\right|_h$ is the amplitude of the harmonic differential current; $\left|\dot{I}_{\varphi Mh}\right|$ is the amplitude of the harmonic current measured on the station side; $\varphi = A, B, C$, λ_{set} is the protection thresholds. Considering the attenuation of characteristic signals in the transmission line, the sensitivity of GFM renewable energy stations to high-resistance grounding faults when connected to a weak system, as well as the boundary of λ_{φ} under internal and external faults, $\lambda_{set} = \frac{\lambda_{max} + \lambda_{min}}{2} = 0.5$. To prevent protection malfunction caused by disturbances such as lightning strikes, an operation command is issued only when Criterion (11) remains continuously valid for 20 ms ; otherwise, the circuit breaker remains closed.

When an internal fault occurs on the transmission line, due to the shunting effect of the fault point, the amplitude of the harmonic current on the station side is larger than that on the system side, $\left|\dot{I}_{\varphi M} + \dot{I}_{\varphi N}\right|_h \approx I_{\varphi Mh}$, λ_{φ} is close to 1. In this case, Criterion (11) is easily satisfied, enabling the protection to operate sensitively. When an external fault occurs on the station side of the transmission line, the short-circuit currents measured on both the station side and the system side are the through currents supplied by the system side. At this time, $\dot{I}_{\varphi Mh} \approx -\dot{I}_{\varphi Nh}$, $\left|\dot{I}_{\varphi M} + \dot{I}_{\varphi N}\right|_h \approx 0$, λ_{φ} is close to 0, so Criterion (11) is not satisfied, and the protection does not operate. When an external fault occurs on the system side of the transmission line, the short-circuit currents measured on both the station side and the system side are the through currents supplied by the station side. At this time, $\dot{I}_{\varphi Mh} \approx -\dot{I}_{\varphi Nh}$, $\left|\dot{I}_{\varphi M} + \dot{I}_{\varphi N}\right|_h \approx 0$, λ_{φ} is close to 0, so Criterion (11) is not satisfied, and the protection does not operate.

4.3. Action Process of Longitudinal Protection

The operation process of the proposed protection scheme is presented in Figure 8.

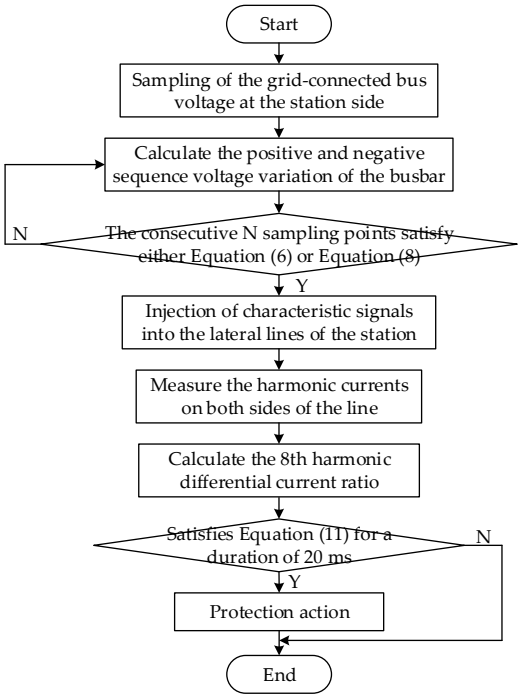

Figure 8. Harmonic current differential protection flow chart based on characteristic signal injection.

 doi:10.20944/preprints202602.2045.v1

5. Simulation Verification and Analysis

A system simulation model, as illustrated in Figure 1, was established in MATLAB/Simulink to verify the performance of the proposed protection scheme. In this model, the capacity of the PV power station is 100 MW, and the transformer on the PV power station side has a turns ratio of 38.5/242 kV with a rated capacity of 120 MW. The outgoing line MN has a length of 40 km and operates at a voltage level of 220 kV. Specifically, F2, F3, and F4 denote internal faults occurring at 25%, 50%, and 75% of the total line length, respectively; F1 represents an external fault on the station side of the transmission line, while F5 indicates an external fault on the system side of the transmission line. The main parameters of the transmission line and the VSG grid-connected system are presented in Table 1.

Table 1. Main parameters of the outgoing line and VSG grid-connected system.

Module Name	Parameter Name	value
Main parameters of the VSG grid-connected system	DC voltage	1500 V
	LC filter inductor	2 mH
	LC filter capacitor	40 μF
	Rated line voltage	690V
	Virtual inertia	105kg·m^2
	Damping	800
Outgoing line	Positive sequence resistance	0.105 Ω /km
	Positive sequence inductor	1.26 mH/km
	Positive sequence capacitor	8.69*10^{-9} F/km
	Zero sequence resistance	0.315 Ω /km
	Zero sequence inductor	3.76 mH/km
	Zero sequence capacitor	6.16*10^{-9} F/km

5.1. Verification of the Injection Control Strategy

At t = 0.3 s, a three-phase metallic grounding fault occurs at the F3 point. The GFM power station starts injecting harmonic current in accordance with the characteristic signal control strategy proposed in Section 3.3. After a system fault occurs, the fault currents measured on both sides of the outgoing line are processed using the Fourier transform algorithm to extract the 2nd to 8th order harmonic components, as presented in Figure 9. Three-phase current waveforms during three-phase metallic phase-to-ground faults and variations of 2nd-8th harmonic currents on both sides of outgoing lines are presented in Figure 9. Figure 9 shows that the characteristic signal injection strategy proposed in this paper can be reliably activated. Furthermore, the PI controller and PR controller are capable of independently regulating the power frequency component and the characteristic signal, respectively.

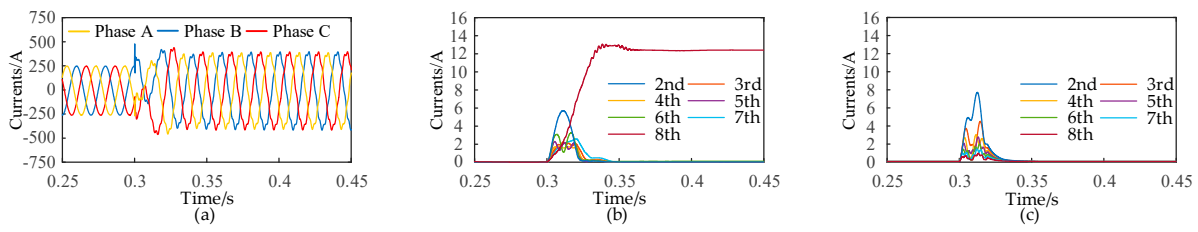

Figure 9. Three-phase current waveforms during three-phase metallic phase-to-ground faults and variations of 2nd-8th harmonic currents on both sides of outgoing lines. (a) Three-phase current waveforms; (b) variations of

 doi:10.20944/preprints202602.2045.v1

2nd to 8th harmonic currents on the station side; (c) variations of 2nd to 8th harmonic currents on the system side.

5.2. Case Study and Analysis

Example 1: At t = 0.3 s, a three-phase metallic grounding fault occurs at Point F3. Following the fault, the positive-sequence voltage at the PCC experiences a sharp drop, thereby triggering the startup criterion for characteristic signal injection. Consequently, the GFM PV power station injects the 8th-order harmonic current into the outgoing line. The current waveforms measured at both ends of the power station's outgoing line before and after the fault are shown in Figure 10. It can be observed that the harmonic components of the station-side current increase significantly after fault inception, whereas the harmonic content on the system side remains relatively low. Meanwhile, the amplitude ratios of the three-phase characteristic signals rise sharply, with the calculated values being $\lambda_A = 1.001$, $\lambda_B = 1.001$, and $\lambda_C = 1.001$, respectively, as illustrated in Figure 10. These values exceed the preset threshold of the protection criterion defined in (11), indicating that the proposed protection scheme operates correctly and reliably under this fault condition.

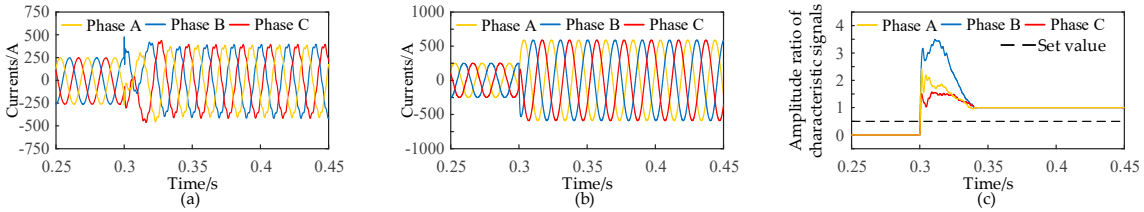

Figure 10. Three-phase currents on both sides of the Line and Action situation of the protection criterion(a) Three-phase current waveforms on the station side; (b) Three-phase current waveforms on the system side; (c) Action situation of the protection criterion.

Example 2: At t = 0.3 s, a three-phase metallic grounding fault occurs at Point F1 outside the protected zone. The calculated amplitude ratios of the three-phase characteristic signals are $\lambda_A = 1\times10^{-5}$, $\lambda_B = 1.4\times10^{-5}$, and $\lambda_C = 1\times10^{-5}$, respectively. These values do not exceed the preset threshold of the protection criterion defined in (11); therefore, the proposed protection scheme does not operate under this external fault condition. Three-phase currents on both sides of the Line and Action situation of the protection criterion are shown in Figure 11.

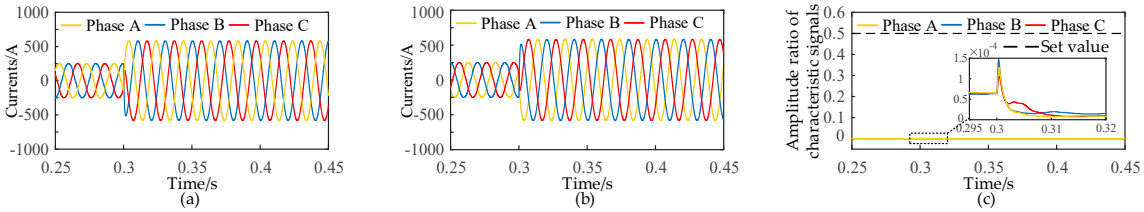

Figure 11. Three-phase currents on both sides of the Line and Action situation of the protection criterion. (a) Three-phase current waveforms on the station side; (b) Three-phase current waveforms on the system side; (c) Action situation of the protection criterion.

Example 3: At t = 0.3 s, a three-phase metallic grounding fault occurs at Point F5 outside the protected zone. The calculated amplitude ratios of the three-phase characteristic signals are $\lambda_A = 0.0001$, $\lambda_B = 0.0001$, and $\lambda_C = 0.0001$, respectively. These values do not exceed the preset threshold of the protection criterion defined in (11); therefore, the proposed protection scheme does not operate under this external fault condition. Three-phase currents on both sides of the Line and Action situation of the protection criterion are shown in Figure 12.

 doi:10.20944/preprints202602.2045.v1

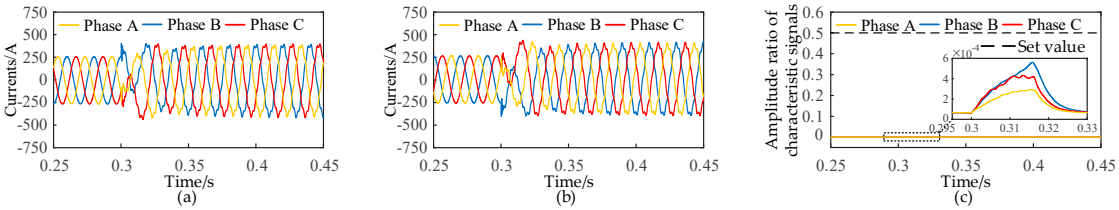

Figure 12. Three-phase currents on both sides of the Line and Action situation of the protection criterion(a) Three-phase current waveforms on the station side; (b) Three-phase current waveforms on the system side; (c) Action situation of the protection criterion.

5.3. Impacts of Different Fault Locations and Fault Types

This section verifies the operating performance of the proposed injection-based protection under various fault conditions. Extensive simulations are carried out with different fault types and locations, both internal and external to the protected line. The corresponding simulation results are presented in Table 2.

Table 2. Different fault types protection operation.

Fault type	Fault location	Amplitude ratio of three-phase characteristic signals			Action situation
		λ_A	λ_B	λ_C	
AG	F2	1.027	0.0011	0.0010	Y
	F3	1.008	0.0004	0.0004	
	F4	0.9829	0.0010	0.0010	
	F1	0.0005	0.0004	0.0003	N
	F5	0.0001	0.0003	0.0003	
BCG	F2	0.0010	1.069	0.962	Y
	F3	0.0004	1.0422	1.0423	
	F4	0.0011	1.012	0.9733	
	F1	0.0004	0.0005	0.0005	N
	F5	0.0003	0.0001	0.0001	
BC	F2	0.0015	1.079	0.8308	Y
	F3	0.0006	1.004	0.8317	
	F4	0.0014	1.147	0.8079	
	F1	0.0004	0.0004	0.0004	N
	F5	0.0004	0.0001	0.0001	
ABCG	F2	1.001	1.007	1.001	Y
	F3	1.001	1.003	1.003	
	F4	1.001	1.001	1.006	
	F1	0.00006	0.00006	0.00006	N
	F5	0.0004	0.0004	0.0004	
ABC	F2	0.9865	0.9862	0.9865	Y
	F3	0.9783	0.984	0.9834	
	F4	0.9789	0.9903	0.9853	
	F1	0.0013	0.0013	0.0013	N

 doi:10.20944/preprints202602.2045.v1

	F5	0.0001	0.0001	0.0001	

As illustrated in Table 2, the injection-based protection scheme proposed in this paper can correctly identify and operate reliably for various fault types both inside and outside the protection zone of the outgoing line.

5.4. Impacts of Different Transition Resistances

This section investigates the transition resistance tolerance capability of the proposed injection-based protection. Tests are performed under A-phase-to-ground faults at various internal fault locations along the line with different transition resistances. The corresponding simulation results are presented in Table 3.

Table 3. Different transition resistances protection operation.

transition resistance	Fault location	Amplitude ratio of three-phase characteristic signals			Action situation
		λ_A	λ_B	λ_C	
0.01	F2	1.04	0.0004	0.0004	Y
	F3	1.015	0.0004	0.0004	
	F4	1.004	0.0010	0.0010	
10	F2	1.022	0.0004	0.0004	Y
	F3	1.008	0.0004	0.0004	
	F4	0.9829	0.0010	0.0010	
50	F2	1.009	0.0005	0.0004	Y
	F3	0.9859	0.0004	0.0004	
	F4	0.964	0.0011	0.0011	
100	F2	0.9669	0.0005	0.0004	Y
	F3	0.9431	0.0005	0.0004	
	F4	0.9152	0.0011	0.0011	
300	F2	0.9005	0.0006	0.0004	Y
	F3	0.869	0.0005	0.0004	
	F4	0.8384	0.0012	0.0011	

As illustrated in Table 3, when the transition resistance reaches 300Ω, the proposed injection-based protection scheme can still operate correctly, exhibiting a strong anti-transition resistance capability.

5.5. Comparison of Operating Performance with Traditional Protection

Based on the aforementioned analysis, the operating performance of the traditional longitudinal differential protection is verified through simulation, taking the GFM renewable energy power station integrated into a weak power grid as the study case. Specifically, a BC two-phase-to-ground fault occurs at Point F4, which is located at 75% of the total outgoing line length within the protection zone, at $t = 0.3$ s, with a transition resistance of 200Ω and a braking coefficient of $K = 0.7$. The operating behavior of the traditional longitudinal differential protection is shown in Figure 13. Under this condition, the traditional longitudinal differential protection fails to operate for both phases B and C.

 doi:10.20944/preprints202602.2045.v1

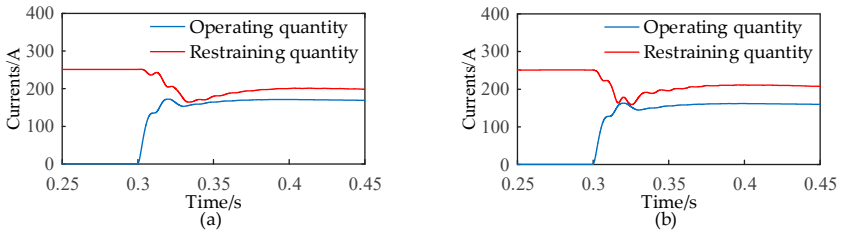

Figure 13. Conditions of traditional longitudinal differential protection action(a) phase B; (b) phase C.

6. Conclusion

In response to the inapplicability issues existing when traditional longitudinal differential protection is applied to the outgoing lines of GFM PV power stations, this paper draws on the design concept of active detection-based protection and proposes a novel active detection-based protection strategy for the outgoing lines of GFM PV stations, which is based on the amplitude ratio of characteristic signals. Through theoretical derivation and simulation verification, the following conclusions are drawn:

1) The proposed protection strategy injects the 8th harmonic into the transmission line and constructs the protection criterion based on the amplitude ratio of the harmonic component of the line differential current to the harmonic component on the power station side. This criterion can quickly and accurately distinguish various faults inside and outside the protection zone of the outgoing line;

2) The proposed protection strategy exhibits excellent anti-transition-resistance capability and can operate reliably under various fault types with stable operating performance;

3) With the amplitude ratio of characteristic signals as its core criterion, the proposed protection strategy has low dependence on phase information, which effectively reduces the requirements for communication synchronization and enhances its engineering practicality.

Although the effectiveness of the proposed protection strategy has been fully veri-fied through theoretical derivation and simulation in this paper, future work will focus on dynamic physical model experiments to further verify the engineering feasibility and practical application effect of the proposed strategy.

Author Contributions: Methodology, Y.L. and C.X.; Validation, Y.L.; Formal Analysis, C.Y., J.C., M.L., and Y.L. All authors have read and agreed to the published version of the manuscript.

Funding: National Natural Science Foundation of China (No. 5236070148).

Data Availability Statement: Data are contained within the article.

Conflicts of Interest: The authors declare no conflicts of interest.

References

1. Song,G.B.; Tao,R.; Li,B.; Hu,J.B.; Wang,C.Q. Survey of Fault Analysis and Protection for Power System with Large Scale Power Electronic Equipment. Automation of Electric Power Systems,2017,41,2-12.
2. Guo,Y.R; Zhou,Z.X.; Liu,Y.; Wang,X.G; Dai,F.Y.; Xu,K. New Principle of Line Differential Protection Based on Combined Current and Voltage Restraint Principle. Proceedings of the CSEE,2025,45,2899-2911.
3. Du,W.J.; Dong,W.K.; Wang,Y. Small-disturbance stability of a wind farm with virtual synchronous generators under the condition of weak grid connection. IEEE Transactions on Power Systems,2021,36,5500-5511.
4. Lin,Y.X.; Li,W.; Zhu,L. Review of transient control strategies for grid-forming converters under grid voltage sag conditions. Electric Power Engineering Technology,2025,44,55-68.
5. Peng,F.; Gao,H.L.; Guo,Y.F. A review of fault ride-through control strategies of grid-forming inverter-based resources and the influence on protection. Power System Technology,2024,48,3673-3685.

 doi:10.20944/preprints202602.2045.v1

6. Xie,H.; Huang,T.; Xu,X.C. Fault characteristic and protection performance under grid-forming control objective. Electric Power Automation Equipment,2024,44,210-216+224.
7. Shi,L.M.; Hui,J.; Tian,B.J. Adaptability analysis of protection for new energy centralized feeders under different control backgrounds. Power System and Clean Energy,2024,40,120-127.
8. Ji,L.; Yu,Z.L.; Li,B.T. Improved VSG control strategy to enhance the adaptability of distance protection. Smart Power,2024,52,9-15+70.
9. Yuan,S.; Ge,Z.; Tang,J.J. Longitudinal protection of grid-forming new energy outgoing lines based on composite sequence current characteristics. Electric Power,2025,58,185-192.
10. Ma,B.Q.; Li,Z.X. A new pilot protection for transmission lines based on overcurrent limiting from grid-forming power sources. Electric Power,2025,58,164-175.
11. Xie,C.; Li,F.T.; Wang,Y.P. An active protection of transmission line based on high-frequency signal. Power System Protection and Control,2017,45,6-12.
12. Dai,Z.H.; Wu,T.; He,J.Y. An active distribution network active injection protection method based on control-protection coordination. Power System Protection and Control,2024,52,94-103.
13. Fang,C.K.; Mu,L.H.; Ou,R. Research on control-protection coordination based on injection protect scheme of microgrid. Proceedings of the CSEE,2023,43,3389-3402.
14. Li,H.F.; Zhang,Z.G.; Liang,Y.S. Current differential protection for distribution network with inverter-interfaced distributed generators based on injection of harmonic signal. Automation of Electric Power Systems,2023,47,120-128.
15. Zhang,Y.B.; Lu,X.J.; Yang,C. Active Injection Pilot Protection for Distribution Network Suitable for Energy Storage Access. Journal of Electrical Engineering ,2025,20,365-378.
16. Yu,S. Research on adaptability analysis methods and new principles for protection of AC transmission lines in renewable energy systems. China Electric Power Research Institute,2024.
17. Liang,Y.Y.; Lu,Z.J. Adaptive differential protection principle based on compensation coefficient for active distribution network. Power System Technology,2022,46,2268-2275.
18. Yao,Z.H.; Dong,W.K.; Han,Z.J. Suppression method for transient voltage fluctuation caused by repeated low voltage ride-through of direct-drive wind turbines. Automation of Electric Power Systems,2025,49,144-152.
19. Li,Z.X.; Li,P.Y.; Xiong,P. Active detection and longitudinal protection of new energy transmission line based on harmonic and composite fundamental ratio. Southern Power System Technology,2025,1-12.